Dynamics of the Anderson impurity model: Benchmarking a nonadiabatic exchange-correlation potential in time-dependent density-functional theory

Niklas Dittmann,[1,2,3] Nicole Helbig,[1,2,4] and Dante M. Kennes[5]

[1]*Institute for Theory of Statistical Physics, RWTH Aachen, D-52056 Aachen, Germany*

[2]*JARA – Fundamentals of Future Information Technology, RWTH Aachen University, D-52056 Aachen, Germany*

[3]*Department of Microtechnology and Nanoscience (MC2), Chalmers University of Technology, SE-41298 Göteborg, Sweden*

[4]*nanomat/Q-MAT/CESAM and European Theoretical Spectroscopy Facility, Université de Liège, B-4000 Liège, Belgium*

[5]*Dahlem Center for Complex Quantum Systems and Fachbereich Physik, Freie Universität Berlin, D-14195 Berlin, Germany*

(Received 8 November 2018; revised manuscript received 24 January 2019; published 13 February 2019)

In this comparative study we benchmark a recently developed nonadiabatic exchange-correlation potential within time-dependent density-functional theory (TDDFT) [Phys. Rev. Lett. **120**, 157701 (2018)] by (a) validating the transient dynamics using a numerically exact density-matrix renormalization-group approach as well as by (b) comparing the *RC* time, a typical linear-response quantity, to up to second-order perturbation theory results. As a test bed we use the dynamics of the single-impurity Anderson model. These benchmarks show that the nonadiabatic potential yields quantitatively accurate results for the transient dynamics for temperatures of the order of the hybridization strength, while the TDDFT *RC* times quantitatively agree with those from second-order perturbation theory for temperatures which are large compared to the hybridization strength. Both results are particularly intriguing given the relatively low numerical cost of a TDDFT calculation.

DOI: 10.1103/PhysRevB.99.075417

I. INTRODUCTION

Nowadays, nonequilibrium quantum many-body physics is at the vanguard of contemporary condensed matter physics. The interest in nonequilibrium phenomena has been stimulated by the ability to conduct controlled experiments, in which external parameters can be influenced with great precision. Several of the first realizations of setups with unprecedented control opportunities were using quantum dots to confine the electrons [1]. Describing quantum-dot experiments out of equilibrium from a theoretical side has hence become a vital field of research. The simplest description of a quantum dot harboring a single energy level employs the so-called Anderson impurity model [2], in which a single spinful degree of freedom is coupled to a Fermi-liquid reservoir of particles [see Fig. 1(a)]. The Anderson impurity model out of equilibrium is the subject of a plethora of theoretical investigations using different tools such as perturbative approaches [3], numerical [4] or density-matrix renormalization-group calculations [5], machine learning *Ansätze* [6], quantum Monte Carlo simulations [7–9], hierarchical quantum master equations [10,11], or time-dependent density-functional theory [12], to name a few. Each of these approaches has its merits as well as shortcomings: Some of them are numerically exact, but difficult to apply to multi-quantum-dot geometries or more complicated couplings (such as spin-orbit coupling), while others employ approximations but tend to generalize more easily.

In order to develop accurate methods for treating more elaborate quantum-dot setups, the approximative approaches require a thorough benchmarking with exact results when possible. This is an important step to establish the range of validity and applicability of the different (and often complementary) methods [13]. In Ref. [12] the authors conduct such a comparison between time-dependent density-functional theory (TDDFT) and the time-dependent density-matrix renormalization group (td-DMRG) (and perturbative methods). The Hartree-exchange-correlation (HXC) potential entering these TDDFT calculations was approximated using an adiabatic local-density approximation, which was motivated from Bethe *Ansatz* insights obtained for the Hubbard model [14,15]. It was shown that this approximation accurately describes the electron density on the quantum dot but steady-state currents are overestimated. The authors conjectured that improvements require the potential to be nonlocal in space and time [12,16].

Recently, in order to improve the performance of TDDFT, a nonadiabatic (i.e., time-nonlocal) approximation for the HXC potential of the single-impurity Anderson model was derived by exploiting analogies to quantum transport theory (see Ref. [17]). The derivation is based on a first-order perturbative treatment in the tunnel coupling between the impurity and the reservoir and uses a Markov approximation for the time propagation in the rate-equation approach. It was shown that the resulting nonadiabatic HXC potential improves over its adiabatic counterpart [18] and yields the correct exponential decay of the density after a quench in the gate voltage [see Fig. 1(b)] [19]. Importantly, directly after the quench, the decay of the density in the TDDFT description deviates significantly from the one obtained with the rate equation. This difference was attributed to the Markov approximation being made in the rate equation while the TDDFT time propagation did not suffer from this additional approximation. However, in TDDFT one propagates the Kohn-Sham system with an approximate HXC potential. Hence, it is not clear which

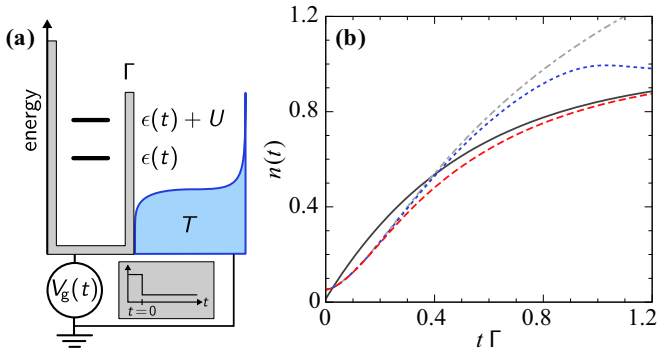

FIG. 1. (a) Sketch of the single-impurity Anderson model at finite temperature T. The single energy level $\epsilon(t)$ with on-site interaction U is tunnel coupled to an electron reservoir with tunnel-coupling strength Γ. The indicated step-pulse gate voltage suddenly shifts the level position at the time $t = 0$. (b) Dynamics after a sudden energy-level shift from $\epsilon(t < 0) = 10\Gamma$ to $\epsilon(t > 0) = -6\Gamma$, with $T = 2\Gamma$ and $U = 16\Gamma$ (figure adapted from Ref. [17]). Shown are TDDFT density evolutions calculated with the nonadiabatic HXC potential from Ref. [17] (long dashed), its adiabatic counterpart [18] (short dashed), and without HXC potential (dashed-dotted lines). The solid line presents a rate-equation result.

of the two methods describes the short-to-intermediate time behavior more accurately.

In the present paper, we benchmark the TDDFT description of this transient dynamics to numerically exact time-dependent DMRG results. While DMRG does provide numerically exact results, it is a low-entanglement method scaling exponentially in the amount of entanglement in the system under scrutiny. In typical quench scenarios, entanglement buildup is linear in simulation time and, as a consequence, numerical resources are exhausted in an exponential fashion. Depending on the prefactor of entanglement growth, this restricts accessible timescales to short-to-intermediate ones. For more complex quantum-dot geometries the overall scaling of numerical cost becomes even worse. In summary, DMRG is the perfect tool for benchmarking the short-to-intermediate time behavior of the nonadiabatic approximation in TDDFT such that we can then address more complex systems within TDDFT with confidence.

As a second test, we compare *RC* times [20] calculated from linear-response TDDFT with those from first- and second-order perturbative treatments in the tunnel coupling [21]. We use this comparison to demonstrate the conceptual difference between perturbation theory on the one hand, and TDDFT employing a HXC potential extracted from perturbative treatments on the other hand. While the HXC potential considered here was derived using only the first order in the tunnel coupling, higher orders can enter due to the exact time propagation of the Kohn-Sham system.

Finally, we note that pushing the boundaries of methods available to describe the dynamics of the Anderson impurity model is relevant also beyond the description of quantum-dot dynamics in experiments. Solutions or high-quality approximations to the quantum-impurity problem out of equilibrium are also urgently needed as impurity solvers in dynamical mean-field theories (DMFTs) and its variances [7], which are nowadays at the frontier of strongly correlated condensed matter research. Especially treating more complicated quantum-dot geometries and spin-orbit coupling is a subject of recently increasing research attention. Furthermore, obtaining a deeper understanding of nonequilibrium physics in general, and specifically the transient response to external changes of quantum dots and beyond, is also crucial to efficiently harvest the promises made by the blossoming field of quantum technologies [22].

The paper is structured as follows: In Sec. II we introduce the Anderson impurity model that is used for all the calculations and present the two methods, time-dependent density-functional theory and density-matrix renormalization-group theory. We discuss the results for the transient dynamics that were obtained with these methods in Sec. III, where we also present the comparison of the *RC* times from TDDFT linear response with those from first- and second-order perturbation theory. We conclude our work in Sec. IV.

II. MODEL AND METHODS

A. Model

As a test bed to benchmark the performance of a recently proposed nonadiabatic HXC potential [17], we consider a single-impurity Anderson model at finite temperature, as depicted in Fig. 1(a).The Hamiltonian is given by

$$H(t) = \sum_{\sigma} \epsilon(t) d_{\sigma}^{\dagger} d_{\sigma} + U d_{\uparrow}^{\dagger} d_{\uparrow} d_{\downarrow}^{\dagger} d_{\downarrow} + \sum_{k,\sigma} \epsilon_k c_{k\sigma}^{\dagger} c_{k\sigma} + \sum_{k,\sigma} (\gamma c_{k\sigma} d_{\sigma}^{\dagger} + \text{H.c.}), \quad (1)$$

where the first, second, and third term describe the isolated impurity, the reservoir, and the reservoir-impurity coupling, respectively. The operators $d_{\sigma}^{(\dagger)}$ annihilate (create) an electron with spin σ on the impurity site while $c_{k\sigma}^{(\dagger)}$ denotes the annihilation (creation) operator for an electron in quasimomentum state k and spin state σ in the reservoir. We neglect the k dependence of the reservoir-dot coupling, i.e., $\gamma_k = \gamma$, for simplicity. The Coulomb repulsion of the electrons on the impurity site is described by the parameter U while the electrons inside the reservoir are treated as noninteracting. The reservoir itself is in thermal equilibrium described by a chemical potential μ, which is set to zero, and temperature T. Since we are not interested in the details of the reservoir, we employ the wideband limit, i.e., we assume that the density of reservoir states ν_0 is a constant. This leads to an energy-independent coupling strength, $\Gamma = 2\pi|\gamma|^2\nu_0$, between the reservoir and the single-impurity site.

We consider two different time-dependent driving schemes for the energy level $\epsilon(t)$: a quench protocol, where $\epsilon(t) = \epsilon(t < 0)\Theta(-t) + \epsilon(t > 0)\Theta(t)$ is rapidly changed from $\epsilon(t < 0)$ to $\epsilon(t > 0)$ at time $t = 0$ by applying a gate voltage, and a low-amplitude harmonic oscillation, $\epsilon(t) = \bar{\epsilon} + A\sin(\omega t)$, around a mean value $\bar{\epsilon}$.

B. Time-dependent density-functional theory

In TDDFT, the interacting system defined in Eq. (1) is simulated by an auxiliary noninteracting—Kohn-Sham (KS)—

system, which has the same electron density as the interacting system. The identical densities are achieved owing to the Hartree (H) and the exchange-correlation (XC) potentials in the KS system, which model electrostatic and all further interaction effects. Along the lines of Ref. [17], we define the KS Hamiltonian for the interacting single-impurity Anderson model of Eq. (1) by

$$H_{\mathrm{KS}}(t) = \sum_{\sigma} [\epsilon(t) + \epsilon_{\mathrm{HXC}}[n](t)] d_{\sigma}^{\dagger} d_{\sigma} + \sum_{k,\sigma} \epsilon_k c_{k\sigma}^{\dagger} c_{k\sigma} + \sum_{k,\sigma} (\gamma c_{k\sigma} d_{\sigma}^{\dagger} + \mathrm{H.c.}), \quad (2)$$

where $\epsilon_{\mathrm{HXC}}[n](t)$ denotes the Hartree and XC contributions. We assume this HXC potential to be a functional of the electron density n on the impurity site. We also neglect XC contributions inside the reservoir, which are known to become relevant for a two-reservoir setup not considered here [23,24].

A modeling similar to Eq. (2) has been used in previous TDDFT studies of the Anderson impurity model, e.g., focusing on the Coulomb blockade [16,25], strong correlation [18], or attractive interaction [26]. In all these works adiabatic potentials were employed for the HXC contribution.

Reference [17] derives a nonadiabatic approximation for the HXC potential of the single-impurity Anderson model by using a reverse-engineering procedure based on perturbation theory in the tunnel coupling in combination with a Markov approximation. The result, which we write as $\epsilon_{\mathrm{HXC}}^{M}(n(t), \dot{n}(t))(t)$, turns out to only depend on the electron density on the impurity site and its first time derivative at time t. It reads

$$\epsilon_{\mathrm{HXC}}^{M}(n(t), \dot{n}(t))(t) = T \log\{C(n(t), \dot{n}(t))\}, \quad (3)$$

with

$$C(n, \dot{n}) = \frac{2e^{U/T}[\dot{n} + \Gamma(n-2)]}{\dot{n} + e^{U/T}[\dot{n} + 2\Gamma(n-1)] - \sqrt{\{\dot{n} + e^{U/T}[\dot{n} + 2\Gamma(n-1)]\}^2 - 4e^{U/T}[(\dot{n} + \Gamma n)^2 - 2\Gamma(\dot{n} + \Gamma n)]}}. \quad (4)$$

A key property of this HXC potential is a smeared-out step at half filling, which becomes a dynamical step for nonzero $\dot{n}(t)$. Both are demonstrated in Fig. 2 for different temperatures, where a lower temperature leads to a sharper potential step [18,25]. Note that the underlying perturbative expansion [3] is justified in the weak-coupling/high-temperature regime, where $\Gamma/T \ll 1$. In this paper, we show that—as long as this constraint is satisfied—TDDFT with the nonadiabatic HXC potential $\epsilon_{\mathrm{HXC}}^{M}$ results in a highly accurate description of the electron dynamics of the single-impurity Anderson model.

In our so-called ensemble TDDFT simulations we propagate the state of the KS system in sufficiently small time steps, and we include a large but finite number of states for the reservoir (see Ref. [17] for technical details). Initially, we begin with a KS system in thermal equilibrium, and we take into account a time-dependent energy level $\epsilon(t)$, which is driven either by a step pulse (Sec. III A) or a low-amplitude harmonic drive (Sec. III B), switched on at time $t = 0$. During the time propagation, the value of $\epsilon_{\mathrm{HXC}}^{M}$ in the KS Hamiltonian changes continuously, based on the evolving electron density. Notably, since the KS system is noninteracting, the numerical cost of these calculations scales linearly in simulation time, which provides an (in general) exponential speed-up compared to numerically exact methods such as, e.g., the density-matrix renormalization-group calculations which we introduce in Sec. II C.

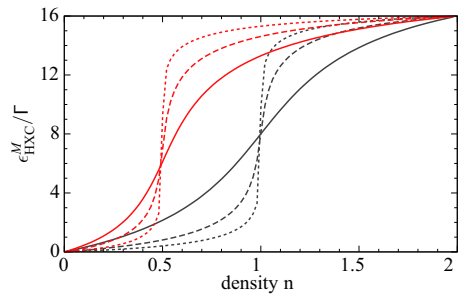

FIG. 2. Nonadiabatic HXC potential $\epsilon_{\mathrm{HXC}}^{M}(n, \dot{n})$ of Eq. (3) for $\dot{n}/\Gamma = 0, 1$ (black and red) and temperatures $T/\Gamma = 4, 2, 1$ (solid, long-dashed, and short-dashed lines). Red lines show the dynamical step appearing for $\dot{n} \neq 0$ [17].

Note that, although it is straightforward from a technical point of view to address more complicated quantum-dot geometries or couplings than the ones considered in this paper, one has to keep in mind that the HXC potential of Ref. [17] was derived using the single-impurity Anderson model. More complicated geometries might call for a modification of this derivation, e.g., in order to include energy-dependent couplings between the quantum dot and the reservoir.

C. Time-dependent density-matrix renormalization group

In many situations, including nonequilibrium setups, interacting one-dimensional systems can be described efficiently using DMRG techniques [27,28]. The model described in Eq. (1) can be mapped onto a one-dimensional linear chain, if we choose to rewrite the structureless reservoir as a nearest-neighbor hopping tight-binding chain, described by hopping amplitude t_h. The resulting reservoir dispersion relation $\epsilon_k = -2t_h \cos(k)$ does not render a structureless reservoir density of states in general, which is integral to compare to the TDDFT results directly. However, if we choose t_h large enough, such that the bandwidth $D = 4t_h$ is much larger than any other energy scale of the system, then the system is effectively in the wideband limit characterized solely by an energy-independent hybridization $\Gamma = 2|\gamma|^2/t_h$. Unfortunately, the large t_h limit is numerically undesirable, because as a consequence of the strong hopping, excitations propagate through the reservoir quickly. As our DMRG (in this nontranslation invariant case) is set up for finite systems, information on the finiteness of

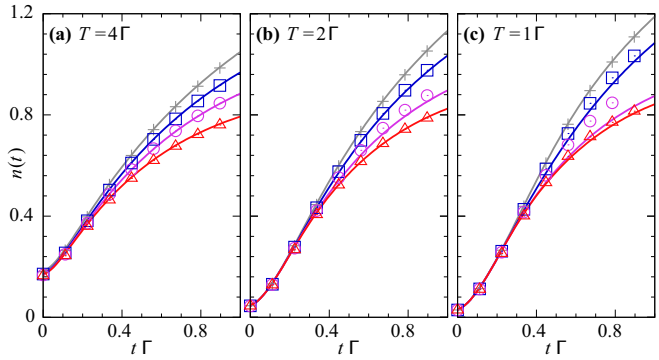

FIG. 3. Comparison of TDDFT densities calculated using $\epsilon^{M}_{\mathrm{HXC}}$ (lines) with DMRG data (symbols). The quantum dot is subject to a quench of the dot's energy level with $\epsilon(t<0)=10\Gamma$ and $\epsilon(t>0)=-6\Gamma$. Top to bottom lines/symbols show different interaction strengths, with $U/\Gamma=0$, 4, 8, 16, and (a)–(c) different temperatures.

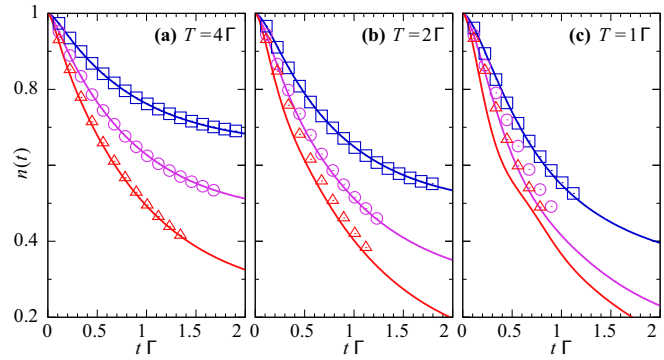

FIG. 4. Comparison of TDDFT densities calculated using $\epsilon^{M}_{\mathrm{HXC}}$ (lines) with DMRG data (symbols) for a quench of the dot's energy level with $\epsilon(t<0)=-U/2$ and $\epsilon(t>0)=U/2$. Top to bottom lines/symbols show different interaction strengths, with $U/\Gamma=4$, 8, 16, and (a)–(c) different temperatures.

the system is imprinted on the dynamics of the impurity on increasingly smaller timescales as t_h is increased. A balance must be struck such that the results are converged with respect to both the wideband limit as well as system size [29]. We checked this convergence by comparing results for different ratios of t_h/γ and reservoir sizes N. We found that choosing $t_h/\gamma=0.05$ and $N=200$ yields converged results and thus used these values for all the DMRG calculations presented here.

To simulate the quench dynamics we employ a two-step procedure. First, we prepare the finite-temperature equilibrium state of Eq. (1) for $H(t<0)$ with $\mu=0$ and a given temperature T using the technique of purification (see Sec. 7 of Ref. [28]). We then employ a real-time evolution algorithm propagating the system with respect to the changed Hamiltonian $H(t>0)$ [30]. In this paper, we use a fourth-order Suzuki-Trotter decomposition with $t_h\Delta t=0.02$, which is small enough to give converged results. The numerical cost of this method scales in an exponential fashion with the entanglement in the system. The control parameter encoding the entanglement growth (and hence the numerical cost) is the so-called bond dimension. In our simulations the bond dimension is dynamically increased during the real-time evolution, such that we obtain numerically exact results. During the simulation the bond dimension generically grows exponentially with simulation time. As a consequence the calculation can only be carried out until the exponential growth exhausts the numerical resources available and no further progress can be made.

III. RESULTS

A. Transient dynamics with TDDFT and DMRG

In this section we present the results of a systematic benchmark of the nonadiabatic HXC potential put forward in Ref. [17] by comparing time-dependent quantum-dot electron densities to numerically exact DMRG data.

Figure 3 summarizes results for a quench of the quantum-dot energy level from a large positive to a negative value, where $\epsilon(t<0)=10\Gamma$ and $\epsilon(t>0)=-6\Gamma$. From left to right the different panels show results for decreasing reservoir temperatures, $T=4\Gamma$, 2Γ, and 1Γ. Different curves in the same panel indicate different interaction strengths U. The TDDFT results are indicated by solid lines, while the DMRG results are shown as symbols. Increasing the interaction from $U/\Gamma=0$ (gray lines and symbols) to finite and strong values, the effects of interactions are clearly discernible for all curves shown. The filling of the initially almost empty quantum dot during the time evolution is hampered by the interaction, on timescales which are not small compared to $1/\Gamma$. The TDDFT results agree very well with the numerically exact results obtained using DMRG up to temperatures as low as $T=2\Gamma$ [see Figs. 3(a) and 3(b)]. These results also justify, *a posteriori*, neglecting the XC effects in the reservoir. For even lower temperatures [see Fig. 3(c)], quantitative deviations are found at times large enough such that the interaction influences the quantum dot's dynamics. The discrepancy between TDDFT and DMRG is largest when the interaction strength is such that the KS energy level after the quench is close to the Fermi energy of the reservoir. We note that the qualitative behavior is in agreement for all interaction strengths and temperatures. We also emphasize once more that, particularly in the beginning of the time evolution, the TDDFT data differ from rate-equation results even in the limit of weak tunneling, as pointed out in Fig. 1(b) [17].

As a second example we consider a quench protocol starting from a half-filled quantum dot and quenching up the energy level, such that charge is dumped into the reservoir. The initially half-filled dot is prepared by choosing $\epsilon(t<0)=-U/2$. The energy level is then quenched to $\epsilon(t>0)=U/2$. Since the strength of the quench is measured in units of U, the noninteracting curve corresponds to performing no quench at all and is thus omitted in the following. From the comparison of the TDDFT and the DMRG data shown in Fig. 4 we conclude a similar picture as found above. As long as the temperature is high enough, the agreement between the two methods is very convincing. Here, we find again that the agreement starts to deteriorate as we approach $T=2\Gamma$, with the deviations increasing with interaction strength and propagation time. Again, the deviations are of quantitative not qualitative nature.

From our results we summarize that the nonadiabatic HXC potential put forward in Ref. [17] can be very useful to describe the transient dynamics of the single-impurity Anderson model, in contrast to TDDFT approaches using adiabatic approximations [18,31], which fail at this task. The regime of quantitative validity, as expected, is restricted to temperature regions which are of the order of Γ. This prohibits access to the strongly correlated Kondo regime of pure spin fluctuations, but nevertheless leaves a large parameter space, where this potential can be applied. This finding is in line with other studies showing that the charge response (at higher T) of quantum-impurity problems is easier to access compared to the the spin response of the system [10,11]. The numerical efficiency of the TDDFT calculations—computational cost scales only linearly instead of exponentially in simulation time—allows one to access systems and timescales beyond state-of-the-art DMRG simulations, including intriguing questions about more complex multidot configurations [17].

Additionally, we point out the success of steady-state density-functional theory (i-DFT) [31–33] to describe strong correlation in the single-impurity Anderson model, which shows that DFT with an accurate XC approximation can be applied even in the Kondo regime. We anticipate that an approximation which combines properties of both the potential of Ref. [31] and the nonadiabatic potential of Ref. [17] opens up a path towards TDDFT simulations of the dynamics in the Anderson impurity model at low temperatures [34].

B. *RC* times with TDDFT and perturbation theory

TDDFT also provides the proper framework to extract linear-response observables from an equilibrium DFT calculation. The HXC potential thereby enters in terms of the HXC kernel. This kernel is calculated from the HXC potential by a functional derivative with respect to the density, which is evaluated at the equilibrium density. In this section, we present a second benchmark of the nonadiabatic HXC potential derived in Ref. [17], focusing on the linear-response dynamics of our system. We compare the derived TDDFT data with perturbation theory in the tunnel coupling in first as well as in second order (see, e.g., Refs. [3,21,35–37]). This comparison highlights the conceptual difference between a perturbation theory description on one hand, and, on the other hand, a TDDFT calculation which employs a HXC potential obtained in perturbation theory.

We investigate a small-amplitude harmonic drive of the energy level $\epsilon(t) = \bar{\epsilon} + A\sin(\omega t)$, around a mean value $\bar{\epsilon}$, and we calculate the finite-frequency admittance $G(\omega) = \frac{\partial I(\omega)}{\partial \epsilon(\omega)}|_{\rm eq}$. Here and in the following, we use the subscript "eq" for all quantities which are evaluated with respect to the equilibrium ($A = 0$) state. As pointed out by Büttiker *et al.* [20], it is instructive to compare the low-frequency part of this admittance to the admittance of a *RC* circuit, which is the classical analog of the system sketched in Fig. 1(a). The low-frequency expansion,

$$G(\omega) \approx -i\omega C + \omega^2 C^2 R, \tag{5}$$

defines a charge-relaxation resistance R and an electrochemical capacitance C for the single-impurity Anderson model. In our benchmark, we compare *RC* times, $\tau_{RC} = RC$, obtained in TDDFT, with results from second-order perturbation theory in the tunnel-coupling strength [21].

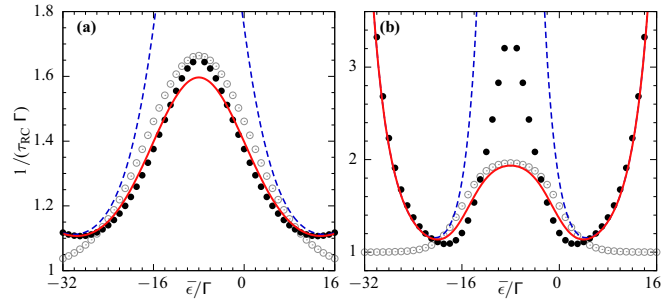

FIG. 5. Inverse *RC* times for two temperatures: (a) $T = 5\Gamma$ and (b) $T = 2\Gamma$. Shown are the *RC* times calculated in TDDFT using the HXC kernels $f^M_{\rm HXC}$ (solid lines) and $f^{\rm ad}_{\rm HXC} = f^M_{\rm HXC}|_{\omega=0}$ (dashed lines), as well as the *RC* times derived in first-order and second-order perturbation theory in the tunnel coupling (open and solid symbols). See also Ref. [21]. The interaction strength is set to $U = 16\Gamma$.

In order to calculate *RC* times in TDDFT, we apply TDDFT linear-response theory. This leads to a Dyson equation for the admittance,

$$G(\omega) = G_{\rm KS}(\omega) + G_{\rm KS}(\omega)\frac{f^M_{\rm HXC}(n_{\rm eq},\omega)}{i\omega}G(\omega), \tag{6}$$

with $G_{\rm KS}(\omega) = \frac{\partial I(\omega)}{\partial \epsilon_{\rm KS}(\omega)}|_{\rm eq}$ denoting the admittance in the KS system. The HXC kernel derived from the nonadiabatic HXC potential of Ref. [17] is here written as [38]

$$f^M_{\rm HXC}(n_{\rm eq},\omega) = f^{(0)}_{\rm HXC}(n_{\rm eq}) - i\omega f^{(1)}_{\rm HXC}(n_{\rm eq}), \tag{7}$$

with $n_{\rm eq}$ being the equilibrium density on the impurity site, and where we abbreviate $f^{(0)}_{\rm HXC}(n_{\rm eq}) = \frac{\partial \epsilon^M_{\rm HXC}(n,\dot{n})}{\partial n}|_{\rm eq}$ and $f^{(1)}_{\rm HXC}(n_{\rm eq}) = \frac{\partial \epsilon^M_{\rm HXC}(n,\dot{n})}{\partial \dot{n}}|_{\rm eq}$. The equilibrium density is obtained by self-consistently solving the density expression $n_{\rm eq} = \frac{\Gamma}{\pi}\int_{-\infty}^{\infty}\frac{f(E)}{(\bar{\epsilon}+\epsilon_{\rm HXC}[n_{\rm eq}]-E)^2+\Gamma^2/4}dE$, with the Fermi function $f(E) = 1/(1+e^{E/T})$. Finally, we insert a low-frequency expansion of $G_{\rm KS}(\omega)$ in Eq. (6) and compare the result with Eq. (5). We find that R and C are connected to the respective values $R_{\rm KS}$ and $C_{\rm KS}$ of the auxiliary KS system by

$$R = R_{\rm KS} + f^{(1)}_{\rm HXC}(n_{\rm eq}), \tag{8}$$

$$C = \frac{C_{\rm KS}}{1 + C_{\rm KS} f^{(0)}_{\rm HXC}(n_{\rm eq})}. \tag{9}$$

Note that the finite-frequency admittance $G_{\rm KS}(\omega)$ and thus $R_{\rm KS}$ and $C_{\rm KS}$ are calculated exactly for the noninteracting KS system [39].

In Fig. 5 we present *RC* times calculated in TDDFT (lines) for two different temperatures as indicated. Let us first focus on Fig. 5(a), where a higher temperature is applied ($T = 5\Gamma$). The TDDFT result based on $f^M_{\rm HXC}$ is plotted as the solid line, and it is compared to first-order as well as second-order perturbation theory results (open and solid symbols) [21]. We observe that the first-order result shows strong deviations compared to the TDDFT data, while the second-order perturbative data agree much better with the TDDFT result over a large range of working points $\bar{\epsilon}$. This is particularly interesting, considering that the underlying HXC potential $\epsilon^M_{\rm HXC}$ is derived

using a first-order perturbative expansion in the reservoir-dot coupling. The reason why the TDDFT data, nevertheless, can match second-order perturbation theory results is that no perturbation theory expansion is employed to solve the KS auxiliary system. Only interaction effects are modeled with a HXC potential motivated from a first-order perturbation theory, while the time evolution in the noninteracting KS system includes all orders in the tunnel coupling. Consequently, deviations between the TDDFT and the second-order perturbation theory data are visible in regions where the interaction plays a more dominant role in the dynamics. In Fig. 5(a), we find that this is the case for working points close to electron-hole symmetry, $\bar{\epsilon} \approx -\frac{U}{2}$. As a further comparison, we also show *RC* times calculated with the adiabatic HXC potential which is related to $\epsilon^M_{\mathrm{HXC}}$ (and which is obtained by setting $\dot{n}$ to zero in the expression for $\epsilon^M_{\mathrm{HXC}}$). These additional data are shown as the dashed line. We find that, when the impurity is close to zero or double occupation, $\bar{\epsilon} \gg 0$ or $\bar{\epsilon} \ll -U$, the adiabatic description suffices, since the interaction plays a subdominant role in these regions. In contrast, the *RC* times are strongly overestimated when the system reaches single occupation.

A similar calculation performed at a lower temperature, $T = 2\Gamma$, is presented in Fig. 5(b). Here, the impact of second-order tunneling on the dynamics is more pronounced. In Fig. 5(b), the limitation of $\epsilon^M_{\mathrm{HXC}}$ is evident: The potential leads to an overfitting of the TDDFT data (solid line) with the first-order perturbation theory result (open symbols), in particular, close to the electron-hole symmetric point [see also the center of Fig. 5(a)]. This result agrees with our findings in Sec. III A, namely, that $\epsilon^M_{\mathrm{HXC}}$ is limited to TDDFT calculations at high temperatures and weak coupling, $\Gamma/T \ll 1$. To also reach lower temperatures, further research is necessary in order to find modifications of this HXC potential which correctly account for interaction effects in this regime.

IV. CONCLUSION

We performed a comparative study in which we benchmarked the validity range of the TDDFT approach based on a nonadiabatic HXC potential put forward in Ref. [17] by comparing to (a) a numerically exact DMRG-based approach as well as (b) results obtained approximately from second-order perturbation theory. In both cases, we found that the accuracy of the nonadiabatic potential is better than expected from its derivation.

By comparing to DMRG we found that the dynamics of a single-impurity Anderson model is accurately described by the proposed nonadiabatic TDDFT approach in the regime of sufficiently high temperature. Therefore, it provides access to the dynamics in this parameter regime by a method that is (at least in general cases) exponentially faster than competitive numerically exact approaches. In other words, the TDDFT calculation does not suffer from the Markov approximation which was made in the derivation of the approximate potential, due to the time propagation of the KS system being numerically exact. However, the low-temperature regime of strongly correlated Kondo physics seems to be off limits to this specific approximation. This agrees with other studies, which demonstrate the relative ease with which the charge response (at higher T) of quantum-impurity problems can be addressed with approximate methods, compared to the spin response of the system [10,11].

In an additional comparison between TDDFT and perturbation theory up to second order, we found a significant increase in agreement between both methods as the second order is included in the perturbation theory. This shows that our TDDFT approach includes important processes of second-order tunneling, although the employed HXC potential was motivated from a first-order calculation. Again, the added accuracy can be ascribed to the exact time propagation of the KS system.

The systematic benchmark of nonadiabatic HXC potentials in TDDFT calculations is the first step along the route to many pressing issues. The reservoir coupled to the single-impurity model imprints relaxation onto the dot degrees of freedom. Including incoherent relaxation processes from scattering in conventional TDDFT simulations proves difficult so far. One way to proxy this relaxation process could be via explicit (and phenomenological) coupling to particle reservoirs as described in this paper. Furthermore, impurity problems as studied here have gained tremendous attention in condensed matter physics, also because of the role they play in dynamical mean-field theory (DMFT). Within the DMFT approach, a (e.g., time-dependent) solution of an impurity problem is required as an input. So far, methods which are able to tackle complicated multiorbital impurities and/or spin-orbit coupling are scarce but urgently needed. Future studies should thus address the issue of multiorbital impurity problems from a TDDFT perspective using nonadiabatic HXC potentials.

ACKNOWLEDGMENTS

We acknowledge funding from the Deutsche Forschungsgemeinschaft via RTG1995 (N.D., N.H.) as well as through the Emmy Noether program (KA 3360/2-1) (D.M.K.). Simulations were performed with computing resources granted by RWTH Aachen University under Projects No. rwth0013 and No. prep0010.

[1] R. Hanson, L. P. Kouwenhoven, J. R. Petta, S. Tarucha, and L. M. K. Vandersypen, Rev. Mod. Phys. **79**, 1217 (2007).
[2] P. W. Anderson, Phys. Rev. **124**, 41 (1961).
[3] J. König, H. Schoeller, and G. Schön, Phys. Rev. Lett. **76**, 1715 (1996).
[4] H. T. M. Nghiem and T. A. Costi, Phys. Rev. Lett. **119**, 156601 (2017).
[5] F. A. Wolf, I. P. McCulloch, and U. Schollwöck, Phys. Rev. B **90**, 235131 (2014).
[6] L.-F. Arsenault, A. Lopez-Bezanilla, O. A. von Lilienfeld, and A. J. Millis, Phys. Rev. B **90**, 155136 (2014).
[7] E. Gull, A. J. Millis, A. I. Lichtenstein, A. N. Rubtsov, M. Troyer, and P. Werner, Rev. Mod. Phys. **83**, 349 (2011).

[8] G. Cohen, E. Gull, D. R. Reichman, A. J. Millis, and E. Rabani, Phys. Rev. B **87**, 195108 (2013).
[9] G. Cohen, D. R. Reichman, A. J. Millis, and E. Gull, Phys. Rev. B **89**, 115139 (2014).
[10] R. Härtle, G. Cohen, D. R. Reichman, and A. J. Millis, Phys. Rev. B **92**, 085430 (2015).
[11] R. Härtle, G. Cohen, D. R. Reichman, and A. J. Millis, Phys. Rev. B **88**, 235426 (2013).
[12] A.-M. Uimonen, E. Khosravi, A. Stan, G. Stefanucci, S. Kurth, R. van Leeuwen, and E. K. U. Gross, Phys. Rev. B **84**, 115103 (2011).
[13] J. Eckel, F. Heidrich-Meisner, S. G. Jakobs, M. Thorwart, M. Pletyukhov, and R. Egger, New J. Phys. **12**, 043042 (2010).
[14] N. A. Lima, M. F. Silva, L. N. Oliveira, and K. Capelle, Phys. Rev. Lett. **90**, 146402 (2003).
[15] C. Verdozzi, Phys. Rev. Lett. **101**, 166401 (2008).
[16] S. Kurth, G. Stefanucci, E. Khosravi, C. Verdozzi, and E. K. U. Gross, Phys. Rev. Lett. **104**, 236801 (2010).
[17] N. Dittmann, J. Splettstoesser, and N. Helbig, Phys. Rev. Lett. **120**, 157701 (2018).
[18] G. Stefanucci and S. Kurth, Phys. Rev. Lett. **107**, 216401 (2011).
[19] Note that the difference between the rate equation and the TDDFT data at the initial time is due to higher-order tunneling, which is partly included in TDDFT but excluded in the rate equation considered here.
[20] M. Büttiker, H. Thomas, and A. Prêtre, Phys. Lett. A **180**, 364 (1993).
[21] J. Splettstoesser, M. Governale, J. König, and M. Büttiker, Phys. Rev. B **81**, 165318 (2010).
[22] F. A. Zwanenburg, A. S. Dzurak, A. Morello, M. Y. Simmons, L. C. L. Hollenberg, G. Klimeck, S. Rogge, S. N. Coppersmith, and M. A. Eriksson, Rev. Mod. Phys. **85**, 961 (2013).
[23] S. Kurth and G. Stefanucci, Phys. Rev. Lett. **111**, 030601 (2013).
[24] Z.-F. Liu and K. Burke, Phys. Rev. B **91**, 245158 (2015).
[25] F. Evers and P. Schmitteckert, Phys. Chem. Chem. Phys. **13**, 14417 (2011).
[26] E. Perfetto and G. Stefanucci, Phys. Rev. B **86**, 081409 (2012).
[27] S. R. White, Phys. Rev. Lett. **69**, 2863 (1992).
[28] U. Schollwöck, Ann. Phys. **326**, 96 (2011).
[29] H. T. M. Nghiem, D. M. Kennes, C. Klöckner, V. Meden, and T. A. Costi, Phys. Rev. B **93**, 165130 (2016).
[30] D. M. Kennes and C. Karrasch, Comput. Phys. Commun. **200**, 37 (2016).
[31] G. Stefanucci and S. Kurth, Phys. Rev. B **97**, 245415 (2018).
[32] G. Stefanucci and S. Kurth, Nano Lett. **15**, 8020 (2015).
[33] S. Kurth and G. Stefanucci, Phys. Rev. B **94**, 241103 (2016).
[34] S. Kurth and G. Stefanucci, Eur. Phys. J. B **91**, 118 (2018).
[35] J. König, J. Schmid, H. Schoeller, and G. Schön, Phys. Rev. B **54**, 16820 (1996).
[36] J. Splettstoesser, M. Governale, J. König, and R. Fazio, Phys. Rev. B **74**, 085305 (2006).
[37] F. Cavaliere, M. Governale, and J. König, Phys. Rev. Lett. **103**, 136801 (2009).
[38] N. Dittmann, J. Splettstoesser, and N. Helbig, J. Phys.: Conf. Ser. **969**, 012145 (2018).
[39] A.-P. Jauho, N. S. Wingreen, and Y. Meir, Phys. Rev. B **50**, 5528 (1994).